

Detection of the Natural Alpha Decay of Tungsten

C. Cozzini^{1,*}, G. Angloher², C. Bucci³, F. von Feilitzsch⁴, D. Hauff², S. Henry¹, Th. Jagemann⁴, J. Jochum⁵, H. Kraus¹, B. Majorovits¹, V. Mikhailik¹, J. Ninkovic², F. Petricca², W. Potzel⁴, F. Pröbst², Y. Ramachers^{1,†}, W. Rau⁴, M. Razeti⁴, W. Seidel², M. Stark⁴, L. Stodolsky², A.J.B. Tolhurst¹, W. Westphal⁴, H. Wulandari⁴

¹*Department of Physics, University of Oxford, Oxford OX1 3RH, U.K.*

²*MPI für Physik, Föhringer Ring 6, 80805 Munich, Germany*

³*Laboratori Nazionali del Gran Sasso, 67010 Assergi, Italy*

⁴*Physikdepartment E-15, TU München, James-Franck-Str., 85748 Garching, Germany*

⁵*Eberhard-Karls-Universität Tübingen, D-72076 Tübingen, Germany*

(Dated: June 12, 2018)

The natural α -decay of ^{180}W has been unambiguously detected for the first time. The α peak is found in a (γ , β and neutron)-free background spectrum. This has been achieved by the simultaneous measurement of phonon and light signals with the CRESST cryogenic detectors. A half-life of $T_{1/2} = (1.8 \pm 0.2) \times 10^{18}$ y and an energy release of $Q = (2516.4 \pm 1.1 \text{ (stat.)} \pm 1.2 \text{ (sys.)})$ keV have been measured. New limits are also set on the half-lives of the other naturally occurring tungsten isotopes.

PACS numbers: 23.60.+e, 07.20.Mc, 29.40.Mc

I. INTRODUCTION

The α -decay of the naturally occurring isotopes of tungsten (W) has been the subject of experimental search for many decades. Tungsten is an interesting element because α -decay is energetically allowed for all five naturally occurring isotopes. Mass excess measurements [1] show that the available decay energy Q for all these isotopes is low (< 3 MeV) and that the Q values lie in the same energy range as β and γ decay due to natural chains (see Table I). Therefore background suppression and possibly event-by-event discrimination against γ 's and β 's, which may obscure the α signal, are crucial issues for the detection of such rare events.

While ^{182}W , ^{183}W , ^{184}W , and ^{186}W are expected to have half-lives well above 10^{32} y, the isotope ^{180}W is ex-

pected to have a half-life near 10^{18} y, and is close to observability with present techniques. Most recently, the Kiev-Firenze Collaboration, operating CdWO_4 scintillation detectors in the Solotvina mine reported a “first indication of a possible α -decay of ^{180}W ” with a half-life of $T_{1/2} = 1.1_{-0.4}^{+0.8}(\text{stat.}) \pm 0.3(\text{sys.}) \times 10^{18}$ years [5]. It is well known [6] that the scintillation yield for α particles is lower than that for β or γ particles of the same energy. After pulse shape analysis, an α -peak at ~ 300 keV was interpreted as ^{180}W α -decay. Due to the low energy resolution (FWHM = 110 keV) it was impossible to exclude alternative explanations for the peak, hence the result was treated as an indication. They also set a 90% C.L. lower limit of $T_{1/2} \geq 0.7 \times 10^{18}$ years. Also the ROSE-BUD collaboration, operating a 54 g CaWO_4 scintillating bolometer at the Canfranc Underground Laboratory, obtained a limit of $T_{1/2} \geq 1.7 \times 10^{17}$ years at 90% C.L [7].

The high sensitivity and excellent energy resolution of low temperature detectors (see for example [8, 10]) and the great efforts made to suppress and understand radioactive background in dark matter searches and double beta decay experiments make such apparatus sensitive to rare nuclear decays. For example, the α -decay of ^{209}Bi (considered as the heaviest stable isotope) has been recently detected by a French group developing low temperatures bolometers for Dark Matter direct detection [11]. CRESST (Cryogenic Rare Event Search with Superconducting Thermometers) is a low background cryogenic facility primarily devoted to the direct detection of WIMP dark matter particles via their scattering by nuclei. Such nuclear recoils resulting from WIMP interaction can be discriminated from electron background (caused by photons or electrons) by measuring phonons and scintillation light simultaneously. The energy detected via phonons in a cryogenic detector is, to first order, independent of the nature of the particle. There is, however, a significant

Isotope	Abundance[%]		Q [keV]	
	IUPAC [3]	Ref. ^a [4]	Ref. [1]	Ref. [2]
^{180}W	0.12(1)	0.1198(2)	2516(5)	2508(4)
^{182}W	26.50(16)	26.4985(49)	1774(3)	1771.8(2.2)
^{183}W	14.31(4)	14.3136(6)	1682(3)	1680.0(2.2)
^{184}W	30.64(2)	30.6422(13)	1659(3)	1656.2(2.2)
^{186}W	28.43(19)	28.4259(62)	1123(7)	1124(7)

^aConsidered by the IUPAC (International Union of Pure and Applied Chemistry) to be the best single measurements.

TABLE I: Representative Isotopic Composition according to the IUPAC, best single measurements on isotopic abundance from individual references, and decay energies for the isotopes of natural tungsten.

*Corresponding author. *Email address:* c.cozzini@physics.ox.ac.uk

[†]Present address: University of Warwick, Coventry CV4 7AL, U.K.

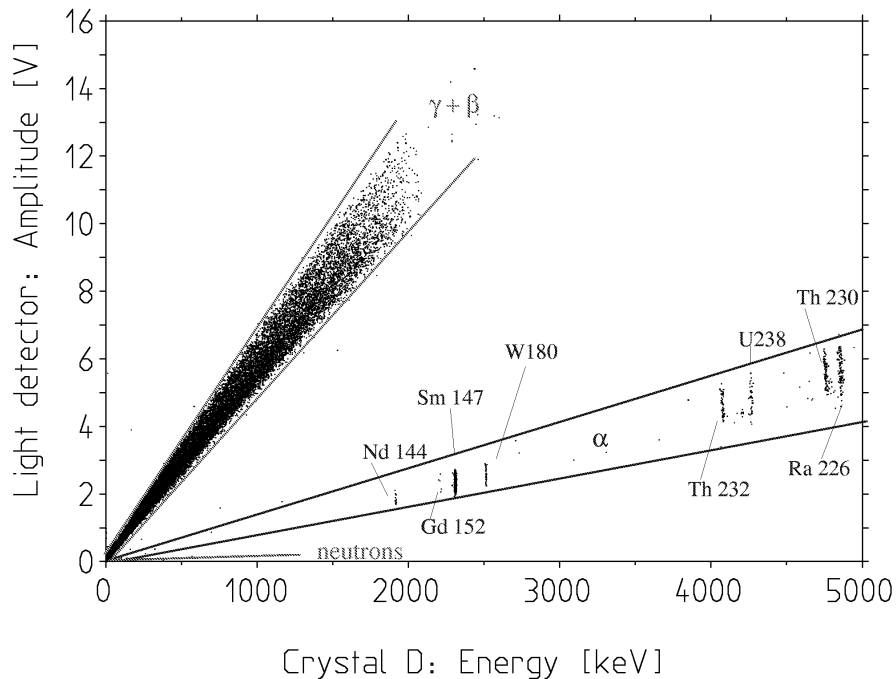


FIG. 1: Pulse amplitude in the light channel versus energy in the CaWO_4 crystal D from run 28. Three clearly separated event populations appear. The solid lines border the three different bands: the upper band is due to γ 's and β 's, the lowest one to neutrons and the middle one is due to α 's. Each peak in the α band has been identified (see text) and is here labelled accordingly.

difference in scintillation yield for nuclei and electrons of the same energy. The fraction of energy released in the nuclear interaction channel, negligible for photons and electrons, becomes important for α 's and heavy ions and is dominant for WIMPs and neutrons. As a result WIMP and neutron induced recoils give considerably less scintillation light than electrons of the same energy while α particles can be clearly discriminated since they interact partly with both, nuclei and electrons. This results in a pure α spectrum, i.e. one without contributions from β, γ and neutron events as in the middle band of Fig. 1. Finally we remark that the energy measured following an internal α -decay in a cryogenic detector corresponds to the sum of the energies of the α particle and of the recoiling nucleus, i.e. the total decay energy Q .

In this paper we present clear evidence for the α -decay of ^{180}W from early runs of the CRESST II dark matter detectors, originating from the tungsten in the CaWO_4 crystals used as the dark matter target.

II. EXPERIMENTAL SET-UP

CRESST is an ultra-low background facility operating at the Gran Sasso underground laboratories. Detailed descriptions can be found in [8, 9]. CRESST has developed very sensitive cryogenic detectors consisting of a dielectric target crystal with a superconducting phase

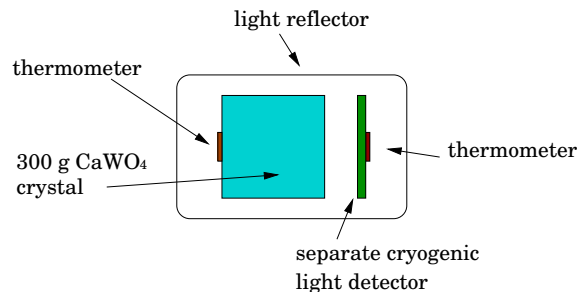


FIG. 2: Schematic of a detector module. It consists of a scintillating 300 g CaWO_4 crystal (phonon channel) and a Si wafer (light channel), both read out by a SPT. The set-up is surrounded by a reflective foil

transition thermometer (SPT) evaporated onto one surface. Particle interactions in a cryogenic detector produce phonons which propagate to the surface, where they heat the electron system in the SPTs. These thermometers, biased in the middle of their superconducting-to-normal transition near a temperature of 10 milli-kelvin, transform the temperature rise of their electrons into a relatively large increase of the resistance of the film. The resistance change of the low impedance thermometer is

then measured via a SQUID. The resistance increase is a measure for the energy deposited.

The set-up for the simultaneous detection of scintillation light and phonons is described in [9] and shown schematically in Fig. 2 for one absorber module. It consists of two independent detectors, each one with its own SPT with SQUID readout. The main detector consists of a $\sim 300\text{g}$ cylindrical CaWO_4 crystal ($\varnothing = 40\text{ mm}$, $h = 40\text{ mm}$). CaWO_4 is a well known scintillator with high light yield and very broad emission spectrum peaked at 420 nm . It is characterized by a high index of refraction ($n = 1.92$) and a decay time of $17\ \mu\text{s}$ at 77 K . The scintillation light produced in each target crystal is detected via an associated calorimeter consisting of a silicon wafer of $(30 \times 30 \times 0.45)\text{mm}^3$ volume with a 20 nm thick SiO_2 layer on both surfaces. In CaWO_4 only a few percent of the absorbed energy is transformed into light. To minimise light losses the whole module is thus enclosed in a highly reflective foil.

In the data to be presented here, three different CaWO_4 crystals (referred to as crystal B, D and E) were used in the Gran Sasso set-up for a total of four different CRESST runs (22, 23, 27, 28). For detector operation, the temperature of the thermometer is controlled by a dedicated heater. Additionally the heater is used to inject test pulses which monitor the long term stability of the detector [9]. In particular, in the runs 27 and 28 a large voltage pulse was produced, reaching the saturation region of the superconducting transition specifically to monitor the detector response above 1 MeV . This pulse was sent, at a rate of 0.5 Hz , throughout the measuring period. A record length of 4096 samples and a time base of $40\ \mu\text{s}$, resulting in a time window of 164 ms for recording an event, was chosen for all the runs presented.

III. OFF LINE ANALYSIS

CRESST detectors are optimised to be most sensitive in the energy region relevant for dark matter direct detection ($<200\text{ keV}$). In this energy range the detector response is mapped out with electric heater test pulses, and the 122 keV line from a ^{57}Co source provides the calibration of the test pulses in terms of a γ equivalent energy [8]. A pulse shape template is obtained by averaging pulses from the 122 keV line. This template is used in a fit to the actual signal pulses in order to accurately determine the signal amplitude. This is valid as long as the detector response is in a linear regime. If the response becomes non-linear the pulse shape changes and the same template cannot be used over the full energy range.

Typically, the pulse shape for the CaWO_4 detectors can be described by $\tau_{\text{rise}} = 1.1\text{ ms}$ and $\tau_{\text{decay}} = 30\text{ ms}$. However, the temperature rise caused by α -decays is usually beyond the dynamic range of the SPT and for precise energy determination the signal duration rather than the pulse height must be used. Therefore two new analysis

methods, described in [12], were developed in order to reconstruct the higher energies (MeV region), for which the detector response is non-linear.

In the first method (Method A) a template from pulses in the linear region (for example the 122 keV template from the calibration) is used to fit all measured pulses with an amplitude below the voltage at which the response becomes non-linear. For all pulses with an amplitude exceeding that voltage the fit is truncated and the upper part is reconstructed from the template. This is shown in Fig. 3. The resulting amplitude spectrum is then linear by construction.

If the pulse duration is too long the information from the decaying part of the pulse is outside the recording time window and the method fails. To overcome this limitation a second method was developed (Method B). The template from the linear region is fitted with a function following the model described in [16]. This assumes an exponential rise and two exponential decay components. Once the parameters of the model function are determined for the linear region, a mathematical description of the changes in pulse shape in the non-linear range is needed. At higher energies the pulse shape varies according to the non-linearities of the superconducting phase transition. These changes can be described via successive approximation to the model function. The higher order correction coefficients are extracted by fitting templates of different energies up to 2.31 MeV (see [12]), enabling the energy spectrum to be reconstructed up to the highest recorded α -signal ($\alpha - \alpha$ cascade at $\sim 15\text{ MeV}$).

IV. BACKGROUND

Due to the powerful discrimination technique CRESST II detectors offer, contaminations from natural decay chains and other α -unstable isotopes have been identified by their α -decays with a sensitivity of $\sim 1\ \mu\text{Bq/kg}$. The results of this analysis have shown very good agreement with the results obtained using different techniques commonly employed to determine the presence of impurities in crystals. These include ICPMS¹ (Inductively Coupled Plasma Mass Spectrometry), HPGe² (High Purity Germanium γ -spectroscopy) and X-ray luminescence³ techniques.

Evidence for contaminations due to α -unstable rare earth elements has been found in all the measured detectors. Rare earth doped crystals are commonly produced for laser applications, therefore these impurities are likely to have been introduced during the production of the crystals. In particular an α peak at 2.31 MeV has been

¹ Gran Sasso Laboratory and Durham University [13]

² Modane Underground Laboratory and Gran Sasso Underground Laboratory [14]

³ Durham University [15]

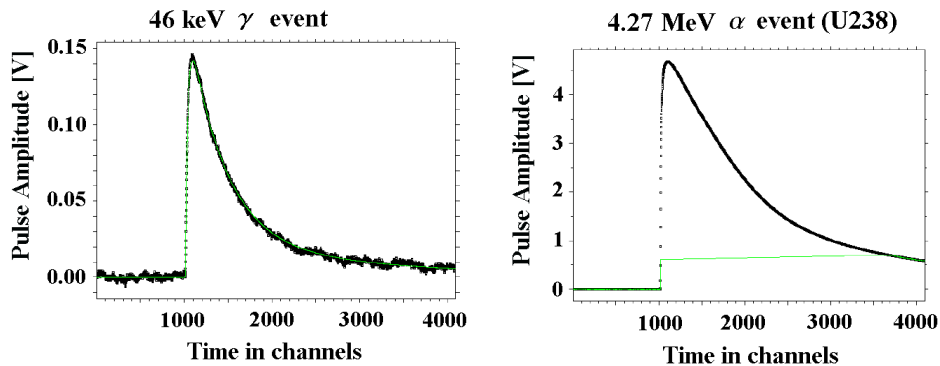


FIG. 3: Fit of two events from crystal D (run 28) with a template obtained by averaging pulses from the 122 keV peak. The fit is truncated at 0.7 V. For pulses of amplitude below this value the fit procedure is standard (left plot). For pulses with an amplitude exceeding this value, the higher part of the pulse shape (above the horizontal dotted line in the right plot) is distorted due to saturation. Therefore the fit is truncated, i.e. fit only to data points below 0.7 V, and the amplitude of the pulse is reconstructed from the template.

	Crystal B				Crystal E
	semi-quantitative analysis		quantitative analysis		semi-quantitative analysis
Natural Element	Sample I [ppb]	Sample II [ppb]	Sample I [ppb]	Sample II [ppb]	[ppb]
Nd	555 ± 167	773 ± 232	683 ± 137	994 ± 199	1100 ± 330
Sm	<22	11 ± 3.3	9 ± 2	13 ± 3	<6
Eu	<8	4 ± 1.2	4 ± 1	5 ± 1	<2
Gd	2898 ± 869	4084 ± 1225			1000 ± 300
Er	1328 ± 398	1877 ± 566			940 ± 283
Dy	<15	<3			<3
Hf	<22	<4			<3
Os	<29	<5			<4

TABLE II: Results from the ICPMS analysis at the Gran Sasso facility on rare earths, hafnium, and osmium. For the semiquantitative analysis the calibration curve is determined with a multi-element standard which may be different from the one to be analysed. On some elements, in particular on samarium, a quantitative analysis was performed. In this cases the calibration is obtained using known standards of the element to be analysed. All the samples are dissolved in a HNO_3 solution in the microwave oven with different exposures for samples I and II.

detected and identified as the α -decay of ^{147}Sm . This isotope is naturally occurring with 15% isotopic abundance and is known to be a pure α unstable radionuclide with $T_{1/2} = 1.06 \times 10^{11}$ years. The intensity of this peak varies for the different detectors, implying different levels of contamination in each crystal. Crystal B showed a count rate of (1.7 ± 0.1) counts/h which translates into (13 ± 1) ppb of natural samarium in the crystal. The rate on the same peak measured with crystal E corresponds to a contamination of (5.5 ± 0.4) ppb of natural samarium.

ICPMS analyses were performed in the Gran Sasso facility on crystals B and E giving results, shown in Table II, in agreement with our analysis of the α -peak intensities. Evidence of ^{144}Nd ($Q = 1905.1$ keV, isotopic abundance (i.a.) = 23.8%, $T_{1/2} = 2.29 \times 10^{15}$ y) and ^{152}Gd ($Q = 2205$ keV, i.a. = 0.2%, $T_{1/2} = 1.08 \times 10^{14}$ y) [18]

α -decay has also been observed and the results are in accordance with the ICPMS analysis. Furthermore, X-ray luminescence analysis on crystal B showed the presence of the characteristic emission peak of Gd and Er [17], the two most abundant rare earth contaminants (see Table II).

Finally, alternative candidates such as ^{174}Hf ($Q = 2496$ keV, i.a. = 0.162%, $T_{1/2} = 2.0 \times 10^{15}$ y) and ^{186}Os ($Q = 2822$ keV, i.a. = 1.58%, $T_{1/2} = 2.0 \times 10^{15}$ y)[18] were considered to cause the 2.31 MeV peak. They were discarded, however, due to the unreasonably high atomic concentration needed to produce the detected rate.

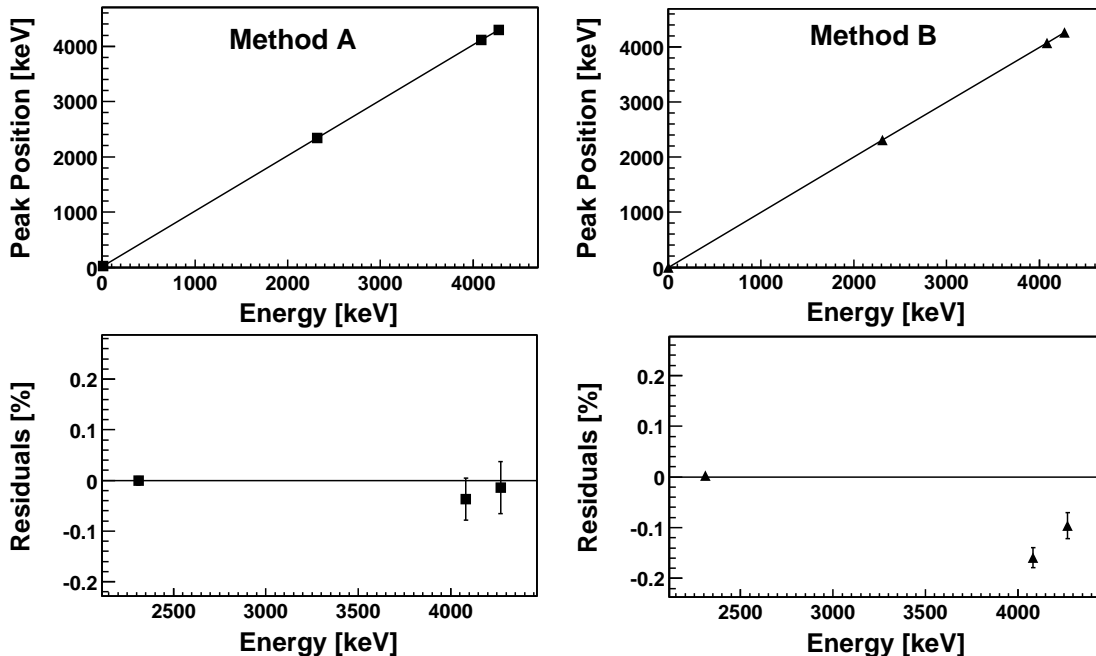


FIG. 4: Top: Fitted peak position versus known energy. The energy scale for the y-axis is fixed by the ^{147}Sm peak while the position of the ^{232}Th and ^{238}U peaks results from a simple linear extrapolation of the calibration for both methods A and B. Bottom: Residuals of the fitted position from the expected position. For method A, the ^{232}Th peak results at (4081.3 ± 1.7) keV ($\Delta E = (28 \pm 4)$ keV (FWHM)) and the ^{238}U at (4269.4 ± 2.2) keV. For method B, the peaks lie at (4076.3 ± 0.8) keV ($\Delta E = (14.1 \pm 1.7)$ keV (FWHM)) and (4265.9 ± 1.1) keV respectively. The calibration of the amplitude spectrum resulting from method A is much more accurate; however, the resolution is less compared with method B.

V. CALIBRATION

Once unambiguously identified, ^{147}Sm was used to calibrate the full α spectrum. This allowed a precise identification of the U-Th peaks, which were then used to determine the accuracy of the calibration for both reconstruction methods A and B. In Fig. 4 the linearity of the response functions for method A (top left figure) and method B (top right figure) is shown for the data of run 28. On the x-axis the central values of the tabulated energies [1] of the ^{147}Sm ($Q = 2310.5 \pm 1.1$ keV), ^{232}Th ($Q = 4082.8 \pm 1.4$ keV) and ^{238}U ($Q = 4270 \pm 3$ keV) peaks are given. On the y-axis their fitted peak position is plotted. The energy scale for the y-axis is fixed on the ^{147}Sm peak at 2310.5 keV while the position of the ^{232}Th and ^{238}U peaks results from a simple linear extrapolation of the calibration. At the bottom of the figure the residuals of the fitted position with respect to the expected position are shown. The calibration of the amplitude spectrum resulting from method A is much more accurate, but less information can be used to reconstruct the signal amplitude compared with method B. This results in a slightly worse energy resolution $\Delta E = (12.9 \pm 0.3)$ keV (FWHM) on the ^{147}Sm peak, and it fails to completely reconstruct the higher part of the U-Th α -spectrum. Method B, on the other hand, using a larger amount of information from the pulses than

method A, gives a much better resolution ($\Delta E = (6.7 \pm 0.1)$ keV (FWHM) on the ^{147}Sm peak), but the approximation of the pulse shape description introduces a higher systematic error on the linear extrapolation of the calibration. In the following, method B has been used to fully reconstruct and identify the entire α spectrum, while method A was applied as an independent check on the peak position of the ^{180}W evidence. In particular, method A is used to extract the measured energy for the ^{180}W Q-value.

VI. RESULTS

Crystal D showed the best performance as a detector (energy resolution: $\Delta E = 1.8$ keV (FWHM) for 122 keV gammas, and $\Delta E = (6.7 \pm 0.1)$ keV for 2.31 MeV alphas, using method B) and it has the longest exposure (11.745 kg days in run 27 and 12.268 kg days in run 28). In run 28 the performance of the module was improved by replacing the Ag reflective foil used in run 27, which showed a ^{210}Pb contamination, by a highly reflective (99% at 420 nm) scintillating polymeric foil. It is these data which we discuss in full detail. A peak was observed at 2512.8 ± 0.4 (stat.) ± 4.3 (sys.) keV with a resolution $\Delta E = (6.5 \pm 0.7)$ keV (FWHM). This is shown in Fig. 5. The position in energy obtained by reconstructing the

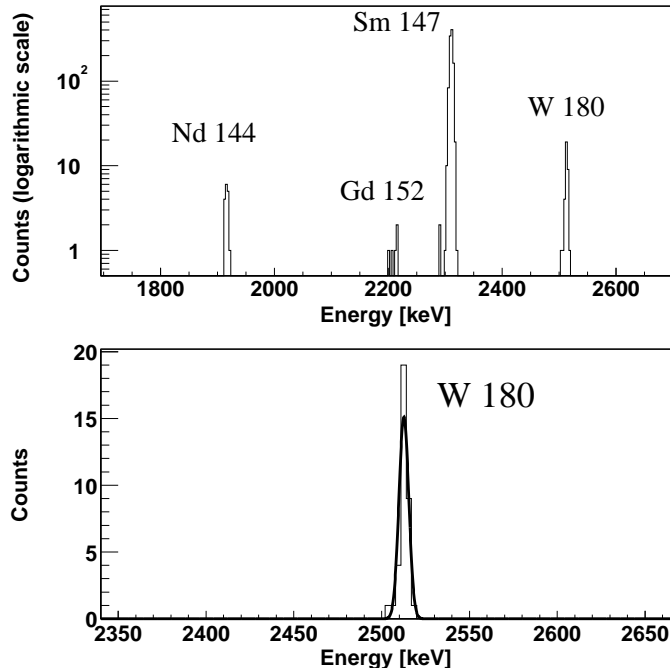


FIG. 5: Alpha events measured in Run 28. In the top figure the energy spectrum between 1.7 and 2.7 MeV is shown with 3 keV bins. On the vertical axis the number of counts are displayed on a logarithmic scale. In the bottom figure the fit to the ^{180}W α -decay is shown. No background counts are present in a wide energy interval around the peak.

spectrum with method A is (2516.5 ± 1.4) keV. A half-life $T_{1/2} = (1.7 \pm 0.2) \times 10^{18}$ y is obtained. This is consistent with the value from run 27 on the same crystal and on crystals B and E, as shown in Table III. The consistency of the results from different crystals tends to confirm that the signal originates from the ^{180}W decay and not from unknown impurities which may be expected to vary for each individual crystal, as seen in Section 4. Furthermore ICPMS measurements performed on these two crystals reported in Table II exclude alternative explanations for the tungsten peak, such as ^{174}Hf .

Finally, the four measurements were added, resulting in a spectrum for a total exposure of 28.62 kg days. The data from each run have been analysed with method A, calibrated individually and then summed. This results in half-life of $T_{1/2} = (1.8 \pm 0.2) \times 10^{18}$ y, which is consistent with the previously published limits. Including the uncertainty on the position of the ^{147}Sm line, a peak of energy $(2516.4 \pm 1.1 \text{ (stat.)} \pm 1.2 \text{ (sys.)})$ keV is found with a resolution $\Delta E = (18 \pm 2)$ keV (FWHM), as shown in Fig. 6. This result is consistent with expectations based on the mass difference of ^{180}W and ^{176}Hf from Ref.[1], but lies 2σ away from the latest update [2] (see Table I). We note however that most of the input data used to evaluate the atomic masses consist of relative measurements which set a relation in mass or energy among two or more nuclei. In the diagram showing the relations among input data (Fig 1 of Ref.[2]), ^{180}W and ^{176}Hf are only weakly connected and an underestimation

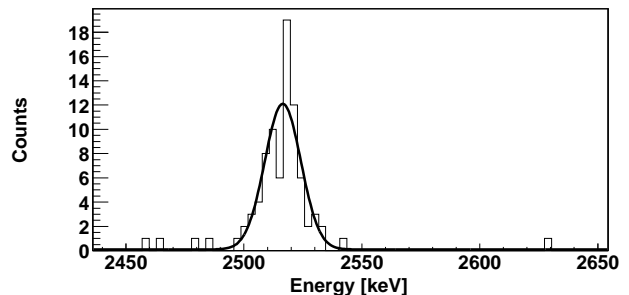


FIG. 6: Sum of the four different runs, each analysed independently with method A. The resulting peak is fitted giving an energy of (2516.4 ± 1.1) keV with resolution $\text{FWHM} = (18 \pm 2)$ keV. Few background events due to a surface contamination of the Ag foil used in run 27 are visible. The scintillating foil used in runs 22, 23 and 28 efficiently vetoes all these events (see text).

of the errors is plausible. Our result represents the missing direct connection between ^{180}W and ^{176}Hf .

Limits on the half-lives for the non-observed α -decays of the other four naturally occurring tungsten isotopes were also calculated. For this purpose the data from run 27 could not be used. In that run, a Ag foil was used to surround the crystal, while in the other three runs the scintillating polymeric foil was used. Any contamination of α -unstable isotopes, such as ^{210}Po on the surface of the

Crystal Run	Exposure	Number	Half-life
number	[kg days]	of counts	[y]
D 28	12.268	35 ± 4.3	$T_{1/2} = (1.7 \pm 0.2) \times 10^{18}$
D 27	11.745	28.5 ± 5.6	$T_{1/2} = (1.9 \pm 0.4) \times 10^{18}$
E 23	3.467	9	$T_{1/2} \geq 1.1 \times 10^{18}$ (90% C.L.)
B 22	1.14	4	$T_{1/2} \geq 6.8 \times 10^{17}$ (90% C.L.)
All Crystals	28.62	75.5 ± 8.7	$T_{1/2} = (1.8 \pm 0.2) \times 10^{18}$

TABLE III: Half-life for the α -decay of ^{180}W obtained from the present work. The results are given independently for the four different runs and for the total exposure. For the runs 27, 28, and the total exposure, the number of counts is determined by a Gaussian fit to the peak. Errors are given at 1σ . For run 22 and 23, due to the small number of counts, the total number of events contained within $\pm 3\sigma$ of the expected energy position is given.

Isotope	Half-life [y]		
	This work	Previous [5]	Previous [7]
^{182}W	$T_{1/2} \geq 7.7 \times 10^{21}$	$\geq 1.7 \times 10^{20}$	$\geq 2.5 \times 10^{19}$
^{183}W	$T_{1/2} \geq 4.1 \times 10^{21}$	$\geq 0.8 \times 10^{20}$	$\geq 1.3 \times 10^{19}$
^{184}W	$T_{1/2} \geq 8.9 \times 10^{21}$	$\geq 1.8 \times 10^{20}$	$\geq 2.9 \times 10^{19}$
^{186}W	$T_{1/2} \geq 8.2 \times 10^{21}$	$\geq 1.7 \times 10^{20}$	$\geq 2.7 \times 10^{19}$

TABLE IV: Lower limits (90% C.L.) on the half-lives of the non-observed α -decays of the other four naturally occurring tungsten isotopes, obtained with a total exposure of 16.875 kg days. For comparison the best previously published limits are also shown [5, 7].

foil or on the crystal may result in α events of degraded energy from the U-Th chain energy, going down to ~ 100 keV. These were observed in run 27 with a rate of 0.087 counts/100keV/kg/day both between ~ 500 keV and the ^{144}Nd peak at 1.9 MeV, and between the ^{180}W and the ^{232}Th peaks. The polymeric foil used in all the other runs did not show any surface contamination. Furthermore if the scintillating side of the foil faces directly the crystal, as in run 28, it efficiently vetoes all the surface events due to the light emitted by the polymeric foil itself. The limits obtained from the sum of runs 22, 23 and 28 are reported in Table IV.

VII. CONCLUSIONS

We have observed the natural α -decay of ^{180}W with a half-life of $T_{1/2} = (1.8 \pm 0.2) \times 10^{18}$ y and a Q-value of $(2516.4 \pm 1.1$ (stat.) ± 1.2 (sys.)) keV. In addition, the lack of any signal from the other tungsten isotopes sets new limits on their half-lives. These results offer an improvement of roughly a factor of 50 over the best previously published limits. Finally we would like to note the power and potential of this cryogenic technique, which here enabled us to achieve a very high sensitivity in an application to nuclear physics.

Acknowledgements

We would like to thank S. Nisi and M. Balata for the ICPMS measurements and M. Laubenstein for the γ spectroscopy analysis at the Gran Sasso Laboratories. Thanks also to C. Goldbach for the Ge measurements at Modane and to the University of Durham for the ICPMS and X-ray luminescence analysis. This work was supported by PPARC, BMBF, the EU Network HPRN-CT-2002-00322 on Applied Cryodetectors, the EU Network on Cryogenic Detectors (contract ERBFM-RXCT980167), the DFG SFB 375 on Particle Astrophysics and two EU Marie Curie Fellowships.

-
- | | |
|---|--|
| <p>[1] G. Audi and A. H. Wapstra, Nuclear Physics A 595 (1995) 409-480.</p> <p>[2] A. H. Wapstra G. Audi and C. Thibault, Nuclear Physics A 729 (2003) 129-676.</p> <p>[3] K. J. R. Rosman and P. D. P. Taylor, Pure and Applied Chemistry 70 (1998) 217.</p> <p>[4] J. Völkening, M. Köppe and K. G. Heumann, International Journal of Mass Spectrometry and Ion Processes, 107 (1991) 361.</p> <p>[5] F. A. Danevich et al., Physical Review C 67 (2003) 014310.</p> <p>[6] J. B. Birks, <i>Theory and Practice of Scintillation Counting</i> (1967), Pergamon, New York.</p> <p>[7] S. Cebrian et al., Physics Letters B 556 (2003) 14-20.</p> <p>[8] G. Angloher et al., Astroparticle Physics 18 (2002) 43-55.</p> | <p>[9] G. Angloher et al., submitted to Astroparticle Physics, astro-ph/0408006.</p> <p>[10] C. Arnaboldi et al., Astroparticle Physics 20 (2003) 91-110.</p> <p>[11] P. de Marcillac, N. Coron, G. Dambier, J. Leblanc, J. Moalic, Nature 422 (2003) 876.</p> <p>[12] F. Pröbst et al., to be submitted.</p> <p>[13] C.J.Ottley, D.G. Pearson and G.J. Irvine in Plasma Source Mass Spectrometry: Applications and Emerging Technologies, edited by J G Holland and S D Tanner, Royal Society of Chemistry, Cambridge (2003) 221-230.</p> <p>[14] C. Arpesella, Nucl. Phys. B (Proc. Suppl.) 28 A (1992) 420.</p> <p>[15] V. B. Mikhailik, I. K. Bailiff, H. Kraus, P. A. Rodnyi and J. Ninkovic, Radiation Measurements 38 (2004) 585-588.</p> |
|---|--|

- [16] F. Pröbst et al., *J. Low Temp. Phys.* 100 (1995) 69.
- [17] J. Ninkovic et al., submitted to *Nucl. Instrum. and Methods A* Proceedings of the SCINT 2003 conference.
- [18] *Table of Isotopes*, edited by R. B. Firestone et al., 8th ed. (1996) Wiley, New York.